Analytical and Bioanalytical Chemistry (2021) 413:3881–3891
https://doi.org/10.1007/s00216-021-03339-y

RESEARCH PAPER

Highly selective fluorescent peptide–based chemosensors for aluminium ions in aqueous solution

Sorour Ramezanpour[1] · Hamed Barzinmehr[1] · Pezhman Shiri[1] · Chris Meier[2] · Seyed Abdulmajid Ayatollahi[3] · Mehrdad Mehrazar[1]

Received: 5 February 2021 / Revised: 7 April 2021 / Accepted: 12 April 2021 / Published online: 30 April 2021

Abstract

Two novel fluorescent peptide–based chemosensors, including **A** (2-amino-benzoyl-Ser-Glu-Glu-NH_2) and **B** (2-amino-benzoyl-Ala-Glu-Pro-Glu-Ala-Glu-Pro-NH_2) were synthesized and characterized by nuclear magnetic resonance (NMR) spectra. These fluorescent probes exhibited excellent selective and sensitive responses to Al^{3+} ions over other metal ions in aqueous buffered solutions. The limits of detection for both chemosensors towards the Al^{3+} ions were in the order of ~10^{-7} M (**A**: 155 nM and **B**: 195 nM), which clearly indicates that these probes have significant potential for biological applications. They also displayed high binding affinity (1.3029×10^4 M^{-1} and 1.7586×10^4 M^{-1} relevant to **A** and **B** respectively). These two chemosensors are great analytical probes that produce turn-on responses upon binding to Al^{3+} ions through an intramolecular charge transfer (ICT) mechanism. In addition, the application of both chemosensors was examined over a wide range of pH. The fluorescent peptide–based probes and Al^{3+} form a 1:1 coordination complex according to the ESI-MS and Job's plot analysis. Notably, upon addition of Al^{3+} to these chemosensors, a fluorescence enhancement of approximately 8-fold was observed and the binding mode was determined using NMR titration and fluorescence emission data.

Keywords Chemosensor · Peptide · Fluorophore · Aluminium · Fluorescence

Introduction

With the growth of society, aluminium compounds are extensively released in the environment and extremely consumed by humans because of excessive utilization of bleached flour, antiperspirants and deodorants, cans, aluminium cookware, antacids and drinking water supplies. Aluminium also plays an essential role in clinical drugs and electrical instruments [1, 2]. The broad usage of Al^{3+} ions results in the accumulation of these ions inside the body [2].

Aluminium ions in high concentrations are very toxic for algae and aquatic plants, fishes, bacteria and other species in aquatic ecosystems. They can also lead to negative impacts on human health. An excess amount of aluminium in the brain tissues may lead to neurological disorders including Alzheimer's disease (AD) and Parkinson's disease (PD). Therefore, the Environmental Protection Agency (EPA) strictly regulated Al^{3+} in surface waters and drinking water to protect human health and the environment [3].

It is critical to detect trace levels of Al^{3+} ions in aqueous media. The selective and sensitive detection of Al^{3+} ions has always been very complicated because of their low coordination with chelating ligands. In recent years, several organic probes which can selectively detect Al^{3+} ions have been reported [4–6]. However, examples of chemosensors for detection of Al^{3+} ions are still less in comparison with chemosensors for detection of other metal ions, mainly owing to the less coordinating ability of Al^{3+} compared with other metal ions [7]. Most reported fluorescent chemosensors also operated in mixed distilled water and organic solutions.

✉ Sorour Ramezanpour
Ramezanpour@kntu.ac.ir

[1] Department of Chemistry, K. N. Toosi University of Technology, P.O. Box 15875-4416, Tehran, Iran

[2] University of Hamburg, Martin-Luther-King Platz 6, 20146 Hamburg, Germany

[3] Phytochemistry Research Center, Shahid Beheshti University of Medical Sciences, Tehran 1434875451, Iran

Thus, the design and synthesis of novel chemosensors for the detection of aluminium ions in aqueous media have attracted considerable attention in analytical chemistry.

Several techniques such as atomic absorption spectrometry (AAS), inductively coupled plasma-mass spectrometry (ICP-MS), voltammetry and potentiometry have been utilized to control and monitor aluminium content under allowable level (7.41 μM) [3, 8–14]. But relatively complicated sample preparation, sample pretreatment protocols and time-consuming procedures are some limitations of these methods. Nowadays, fluorescent chemosensors are excellent tools for the determination of Al^{3+} ions, owing to their high sensitivity, low detection limits, fast responses, non-destructive analysis and inexpensive small instrumentation.

Previous studies have emphasized the importance of the combination of amino acids or short peptides with conjugated fluorophores on the detection of transition metal ions due to their strong metal-binding affinity, water solubility and biocompatibility [15, 16]. Peptides are an ideal option for the design of ion-selective probes to perform fluorescence measurement experiments in aqueous media as well. However, there have been a few attempts for the design and preparation of fluorescent peptide–based chemosensors [17–22].

Lee and co-workers reported a fluorescent sensor based on a tripeptide (SerGluGlu) with a dansyl fluorophore for the selective detection of Al^{3+} among 16 metal ions in aqueous buffered solutions with a detection limit of 230 nM [3].

In this article, we aim to report the synthesis of two fluorescent peptide–based chemosensors, including **A** (2-amino-benzoyl-Ser-Glu-Glu-NH_2) and **B** (2-amino-benzoyl-Ala-Glu-Pro-Glu-Ala-Glu-Pro-NH_2) and their application in selective detection of Al^{3+} ions in aqueous solution with low detection limits (Scheme 1). These chemosensors have been designed on the basis of the ICT mechanism and displayed fluorescence turn-on responses upon binding to Al^{3+} ions. Both fluorescent peptide–based chemosensors contain N- and O-donors which provide a hard base environment for hard acid Al^{3+} ions [23–25]. According to Fig. 1, the attachment of a guest species to the donor moiety reduces the donating nature, resulting in a decreased ICT effect and fluorescence quenching. On the other hand, binding to the withdrawing moiety strengthens ICT intensity and leads to fluorescence emission enhancement. In the former case, the HOMO-LUMO gap of energy increases and a blue shift is observed. In the latter case, the HOMO-LUMO gap of energy decreases and a red shift occurs [26–31]. According to Scheme 1, either of the chemosensors interacts with aluminium ions through the amide group (i.e. the electron-withdrawing group) that increases fluorescence intensity up to 8-fold. There must be an electronic system composed of an electron donor moiety, an electron-withdrawing moiety and a π-conjugated system to proceed via an ICT mechanism. Both chemosensors contain 2-amino benzoyl moiety as the fluorophore with amino group, being the donor moiety. In addition, the amide group of the first amino acid attaching to 2-amino benzoyl acts as the

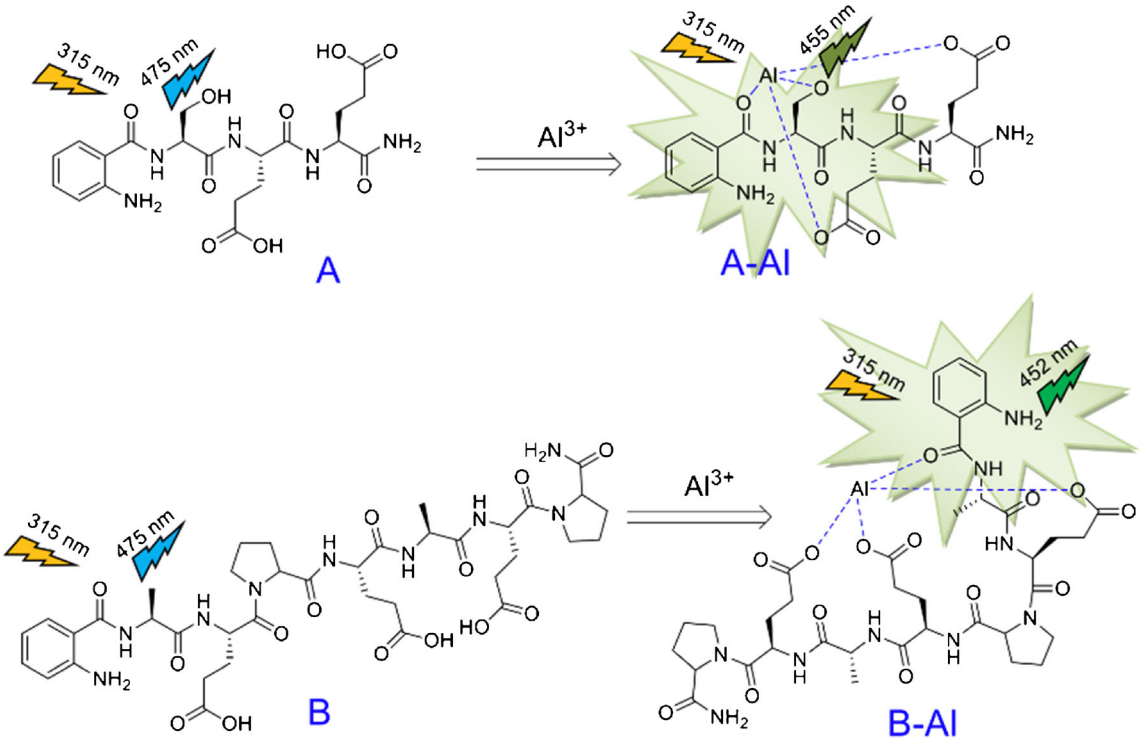

Scheme 1 Structures and proposed binding modes of **A** and **B**

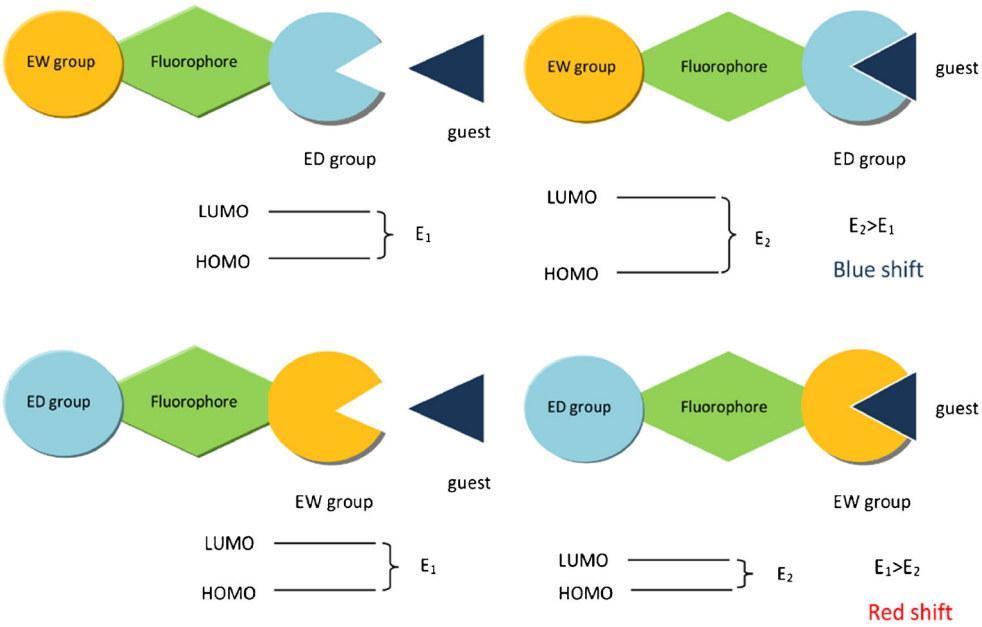

Fig. 1 Illustration of ICT mechanism in a fluorescent chemosensor

electron-withdrawing group [32, 33]. According to Scheme 1, either of chemosensors interacts with aluminium ions through the amide group (i.e. the electron-withdrawing group) that increases fluorescence intensity up to 8-fold. The logic behind the design of chemosensor **A** is a simple fluorophore replacement on the successful aluminium sensing peptide sequence reported by Lee and co-workers. The substitution of isatoic anhydride which is a cheaper and more water-soluble reagent than dansyl chloride proffered lower detection limit as well. Chemosensor **B** was designed based on a natural peptide sequence found in Apidaecin 1 gene peptide (Ala-7-pro). This natural sequence drew our attention due to its three glutamic acids which could provide the ligating sites for Al^{3+} and its pro residues with twisting ability which would potentially kink the heptapeptide, trapping aluminium ions as did the tripeptide chain of **A**. The kink provided by pro residues was confirmed by the optimization of structures of **A** and **B** before and after binding to Al^{3+} [34–38].

Materials and methods

Reagents

All the reagents, including Fmoc-Ser-(tBu)-OH, Fmoc-Glu-(OtBu)-OH, Fmoc-Ala-OH, Fmoc-Pro-OH, isatoic anhydride, Rink amide MBHA resin, 2-(1H-benzotriazole-1-yl)-1,1,3,3-tetramethyluronium tetrafluoroborate (TBTU), dichloromethane (DCM), N,N-dimethylformamide (DMF), piperidine, trifluoroacetic acid (TFA), ethanol, methanol, ninhydrin, triethylsilane (TES) and N,N-diisopropylethylamine (DIEA), were purchased from Merck. All solvents were of analytical reagent grade. Stock solutions of Al^{3+}, Ga^{3+}, Ni^{2+}, Cd^{2+}, Ca^{2+}, Ag^{+}, Pd^{2+}, Mg^{2+}, Mn^{2+}, Fe^{2+}, Cr^{3+}, Fe^{3+}, Cu^{2+}, Zn^{2+}, Hg^{2+} and Co^{2+} with perchlorate anion as well as Na^{+} and K^{+} with chloride ion were prepared by double-distilled water (ddH_2O). All fluorescence measurements were also performed with double-distilled water.

Materials

Absorption spectra were determined with a Unico UV-4802 spectrophotometer. Fluorescence measurements were performed on a PerkinElmer LS50B luminescence spectrometer and the lifetime measurements of the samples were carried out on an Edinburgh Instrument FSL920. The pH measurements were carried out using a SAT-401 Auto Cal pH meter. ^1H NMR spectra were recorded using a Bruker 400MHz spectrometer and electrospray ionization mass spectra (ESI-MS) were recorded on a Mass-ESI-POS (ApexQe-FT-ICR instrument) spectrometer. Samples were freeze-dried on a Martin Christ alpha 1-2 LDplus and crude products were purified using a Knauer preparative HPLC (Eurospher 100-10 C18, column 250 × 16 mm) instrument. The purity of final products was also ascertained using a Knauer analytical HPLC with a ODS C18 column.

Solid phase synthesis of A and B

Both **A** and **B** were synthesized by solid phase synthesis method with Fmoc chemistry. For the synthesis of **A**, Fmoc-Glu(OtBu)-OH (680 mg, 1.6 mmol) was resembled on swollen, deprotected Rink amide MBHA resin (1 g). After deprotection of the Fmoc protecting group from the resin bound Glu, Fmoc-Glu(OtBu)-OH (680 mg, 1.6 mmol) and Fmoc-Ser(tBu)-OH (610 mg, 1.6 mmol) were coupled

successively. Following deprotection of the Fmoc group, isatoic anhydride (260 mg, 1.6 mmol) was coupled to the resin bound tripeptide. DIEA (0.48 mL, 2.8 mmol) and TBTU (510 mg, 1.6 mmol) were used for each coupling step (Scheme S1). The chemosensor **B** was synthesized with a similar method. First, Fmoc-Pro-OH (270 mg, 0.8 mmol) was attached to the swollen Rink amide MBHA resin (1 g). After deprotection of the Fmoc group from the resin bound Pro, Fmoc-Glu(OtBu)-OH (0.34 g, 0.8 mmol), Fmoc-Ala-OH (0.25 g, 0.8 mmol), Fmoc-Glu (OtBu)-OH (0.34 g, 0.8 mmol), Fmoc-Pro-OH (270 mg, 0.8 mmol), Fmoc-Glu(OtBu)-OH (0.34 g, 0.8 mmol) and Fmoc-Ala-OH (0.25 g, 0.8 mmol) were successively coupled. After deprotection of the Fmoc group from the resin bound heptapeptide, isatoic anhydride (0.13 g, 0.8 mmol) was finally coupled. For each coupling step, DIEA (0.24 mL, 1.4 mmol) and TBTU (0.26 g, 0.8 mmol) were added. All deprotection steps were carried out with 25% piperidine in DMF and after every coupling and deprotection step, the resin was washed three times with DMF (5 mL) and DCM (5 mL). After the completion of the synthesis, the resin was dried with pumps and then the cleavage of peptides from the resin was performed using a solution of 10.8 mL TFA/H_2O/MeOH/TES (92:3:3:2 v/v/v/v) at room temperature for 4 h (Scheme S2). The crude products were triturated with diethyl ether, chilled at −20 °C and centrifuged at 5000 rpm for 5 min at 10 °C. After that, **A** and **B** were purified with preparative HPLC with a C18 column using a water (1% TFA)-acetonitrile (0.2% TFA, 19.8% H_2O) gradient to yield 72% of **A** and 81% of **B**. Then, the purity and structure of both products were ascertained by using analytical HPLC with a C18 column (>98% both **A** and **B**) (see Supplementary Information (ESM) Figs. S1 and S2) and ESI-mass spectrometry (ESM Figs. S3 and S4).

Absorbance and fluorescence measurements

Absorbance data were recorded using a UNICO UV-4802 model spectrophotometer and a PerkinElmer LS-50B luminescence spectrometer was used to record emission data. A stock solution of **A** (1 mM) and a stock solution of **B** (1 mM) were prepared and stored in a dark place at −20 °C. All fluorescence and absorbance measurements were performed using these solutions in the presence of 10 mM hexamine buffer without any co-solvent. Emission and absorbance measurements were conducted at pH 5.5 in 10-mm path length quartz cuvette. Absorbance spectra of **A** and **B** were recorded in the presence of eighteen metal ions including Al^{3+}, Ga^{3+}, Ni^{2+}, Cd^{2+}, Ca^{2+}, Ag^{+}, Pd^{2+}, Mg^{2+}, Mn^{2+}, Fe^{2+}, Cr^{3+}, Fe^{3+}, Cu^{2+}, Zn^{2+}, Hg^{2+}, Co^{2+} with perchlorate anion and Na^{+}, K^{+} with chloride ion at an excitation wavelength of 315 nm according to Figs. S10 and S11 (see ESM). The slit widths for both excitation and emission were 10 nm.

Binding constants of A-Al and B-Al

The association constants for 1:1 complex of **A**-Al ($1.3029 \times 10^4\ M^{-1}$) and **B**-Al ($1.7586 \times 10^4\ M^{-1}$) were calculated based on the linear least-squares fit of the titration data and using the following equation (modified Benesi-Hilderbrand equation) [39–41] (ESM Figs. S14 and S15):

$$\frac{1}{F-F_{\min}} = \frac{1}{K[\mathrm{M}](F_{\max}-F_{\min})} + \frac{1}{(F_{\max}-F_{\min})}$$

where $F_{\min}$, F and $F_{\max}$ denote the emission intensities of the chemosensor in the absence of Al^{3+} ions, at an intermediate aluminium concentration and at a concentration of maximum interaction, respectively. [M] is the concentration of Al^{3+} and K is the binding constant. The experiment was performed in double-distilled water in the presence of 10 mM hexamine buffer with variable concentration of Al^{3+} (0–50 μM).

Detection limit of A and B for Al^{3+}

The limit of detection (LOD) was determined based on fluorescence titration by using the following equation:

$$\mathrm{LOD} : 3\delta/m$$

where δ is the standard deviation of the blank and m denotes the slope of a plot of fluorescence intensity against aluminium concentration. δ was determined by measuring fluorescence intensity of 10-μM solutions of **A** and **B** 10 times in the absence of metal ions. m was also obtained by plotting fluorescence intensity of 10-μM solutions of **A** and **B** against variable concentrations of Al^{3+} (0–50 μM) in double-distilled water in the presence of 10 mM hexamine buffer. According to Figs. S12 and S13 (see ESM), LODs of **A** and **B** are 195 and 155 nM, respectively.

Lifetime and quantum yield

In the presence of Al^{3+}, quantum yields of **A** (0.04723) and **B** (0.04658) in HEPES buffer increased up to 0.14169 and 0.15705 respectively and both chemosensors exhibited strong fluorescence emission. Quantum yield (ΦF) was determined in hexamine buffer with reference to an anthracene standard using the following equation:

$$\Phi = \Phi_{\mathrm{R}}\left(\frac{m}{m_R}\right)\left(\frac{n^2}{{n_R}^2}\right)$$

where m is the slope of the line obtained from the plot of the integrated fluorescence intensity versus absorbance and n is the refractive index of solvent. The lifetime measurements of the samples were also performed on an Edinburgh Instrument FSL920. The average lifetime was determined using the following equation:

$$< \tau >= \frac{\sum A_i \tau_i^2}{\sum A_i \tau_i}$$

where τ and A are the lifetime and amount of each component respectively (ESM Figs. S19 and S20).

Identification of A and B

The ^{1}H NMR data were recorded on a Bruker Ascend 400 MHz instrument and Mass-ESI-POS (Apex Qe-FT-ICR) instrument was used to determine the molecular weights of final products (**A**, **B**, **A**-Al and **B**-Al) (ESM Figs. S5–S8).

Results and discussion

Fluorescence response of A and B to metal ions

Al^{3+} strongly interacts with hard donor ligands (e.g. carboxylate group of Glu side chain and hydroxyl group of Ser side chain), owning to its hard acidic nature. Hence, it is estimated that **A** and **B**, bearing Glu and Ser amino acids, would be able to selectively sense Al^{3+} at the excitation wavelength of 315 nm [42, 43]. This hypothesis was confirmed by measuring the fluorescence intensity of **A** and **B** in the presence of 5 equiv of eighteen perchlorate salts of metal ions, including Al^{3+}, Ga^{3+}, Ni^{2+}, Cd^{2+}, Ca^{2+}, Ag^{+}, Pd^{2+}, Mg^{2+}, Mn^{2+}, Fe^{2+}, Cr^{3+}, Fe^{3+}, Cu^{2+}, Zn^{2+}, Hg^{2+} and Co^{2+} and 5 equiv of two chloride salts of Na^{+} and K^{+} 10 mM hexamine buffer at pH 5.5.

Among tested metal ions, only Al^{3+} could enhance emission intensity of **A** up to 7.4-fold and **B** up to 8.3-fold. Ga^{3+} ions could approximately enhance emission intensity of chemosensors up to 3-fold as well. However, both chemosensors displayed stronger affinity for aluminium ions.

As shown in Fig. 2, sensors **A** and **B** displayed a maximum fluorescence emission at 475 nm (λ_{em} = 475 nm). The addition of Al^{3+} ions induced blue shifts from 475 to 455 nm and 475 to 452 nm for **A** and **B**, respectively. These blue shifts are observed because non-bonding molecular orbitals achieve more stability during the binding event. Furthermore, the addition of aluminium ions produced turn-on responses, enhancing the emission intensity. The binding of Al^{3+} with the amide group of 2-amino benzoyl (the electron-withdrawing moiety) strengthens the withdrawing nature which leads to greater intensity of $\pi \rightarrow \pi^*$ electronic transitions (greater ICT), producing higher fluorescence emission. According to Fig. 3, 5 equiv of Al^{3+} ions was required to saturate fluorescence response of **A** and **B** [44–46].

Fluorescence titration of A and B with Al^{3+}

As shown in Fig. 3, fluorescence emissions of **A** (10 μM) and **B** (10 μM) were measured in the presence of varying concentrations of Al^{3+} (0, 5, 10, 15, ……. and 60 μM) in 10 mM hexamine buffer at pH 5.5. Excited at 315 nm, both chemosensors displayed maximum emission at 475 nm. Fluorescence emission was enhanced with increasing aluminium concentration up to 50 μM (5 equiv), resulting in 7.4-fold enhancement of **A** with a 20-nm blue shift and 8.3-fold enhancement of **B** along with a 23-nm blue shift. Higher concentrations caused no change in emission intensity, leading to a constant line in the graph.

The effect of pH and buffering agent on fluorescence emission

Considering an ICT process as the electron transfer mechanism, pH effects on fluorescence spectra are predictable. In

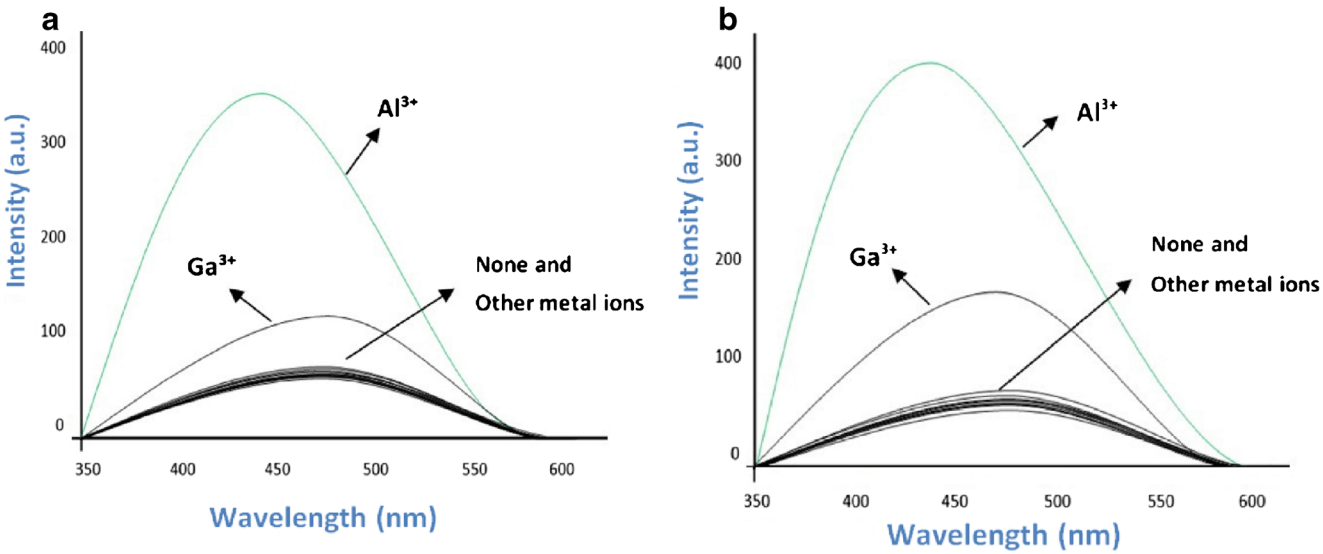

Fig. 2 Fluorescence responses of 10 μM of **A** and **B** to metal ions in the presence of 5 equiv of various metal ions by an excitation wavelength at 315 nm in 10 mM hexamine buffer at pH 5.5. (a) Fluorescence emission spectra of **A**. (b) Fluorescence emission spectra of **B**

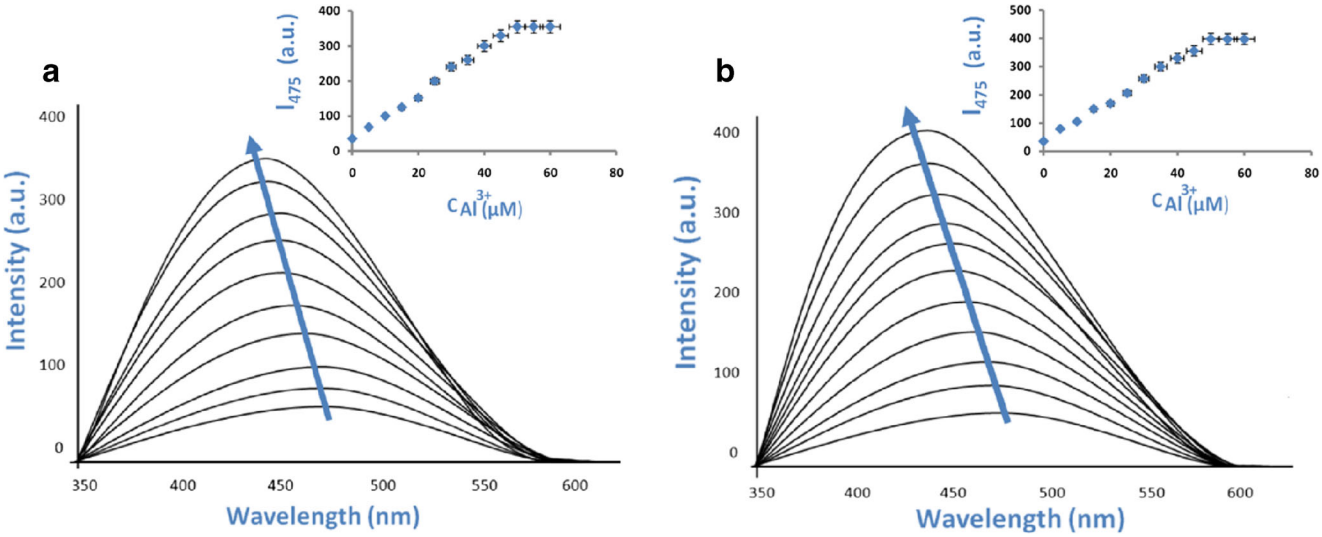

Fig. 3 (a) Fluorescence emission spectra of **A** (10 μM) in 10 mM hexamine buffer with increasing concentrations of Al^{3+} (0, 5, 10, . . . 60 μM) at pH 5.5. (b) Fluorescence emission spectra of **B** (10 μM) in 10 mM hexamine buffer following addition of Al^{3+} (0, 5, 10, . . . 60 μM) at pH 5.5

acidic pH < 4, **A** and **B** display very weak fluorescence due to the protonation of the amino group on 2-amino benzoyl moiety and blockage of the ICT process. For 4 < pH < 7, emission intensity reaches the maximum. At neutral pH, aluminium ions might be hydrated to form insoluble $Al(OH)_3$ that does not interact with the ligands in aqueous solution. At pH > 8, $Al(OH)_4^-$ ions as negative species are formed and the resultant electrostatic repulsion with carboxyl groups on **A** and **B** prevents Al^{3+} from binding to the chemosensors. As shown in Fig. 4, both chemosensors exhibited highest emission intensity at pH 5.5. Therefore, all tests were performed at this pH. Other buffering agents were examined as well. HEPES and phosphate buffers are two of the most common buffered solutions reported in peptide-based chemosensors that were tested. Phosphate buffer with a pH range of 5.8 to 8 and HEPES buffer with a pH range of 6.8 to 8.2 did not cover the optimal pH range. HEPES buffer did not afford higher intensities than 220 a.u. As for phosphate buffer, high intensities of 345 a.u. for **A**-Al and of 385 a.u. for **B**-Al were observed at pH 5.8. However, phosphate buffer did not allow the examination of pH in more acidic conditions. In addition, compared with phosphate buffer, use of hexamine buffer led to higher intensities for pH > 6. Hexamine buffer with pH values ranging from 2.8 to 7 proved to be the best buffering agent that allows the measurement of fluorescence at pH 5.5, pH < 5.5 and pH > 5.5 [47–50].

Fluorescence interference test

The emission intensity of **A** and **B** in the presence of Al^{3+} and other metal ions was measured to investigate the interference effect. As presented in Fig. 5, the blue bars show that when Al^{3+} is the only metal ion to bind, there is such a strong emission. In the presence of both Al^{3+} and other metal ions, there is still high fluorescence intensity and except for 4 metal ions, including Cr^{3+}, Hg^{2+}, Fe^{3+} and Cu^{2+}, all other metal ions afforded high intensities over 300 au that indicates the high aluminium

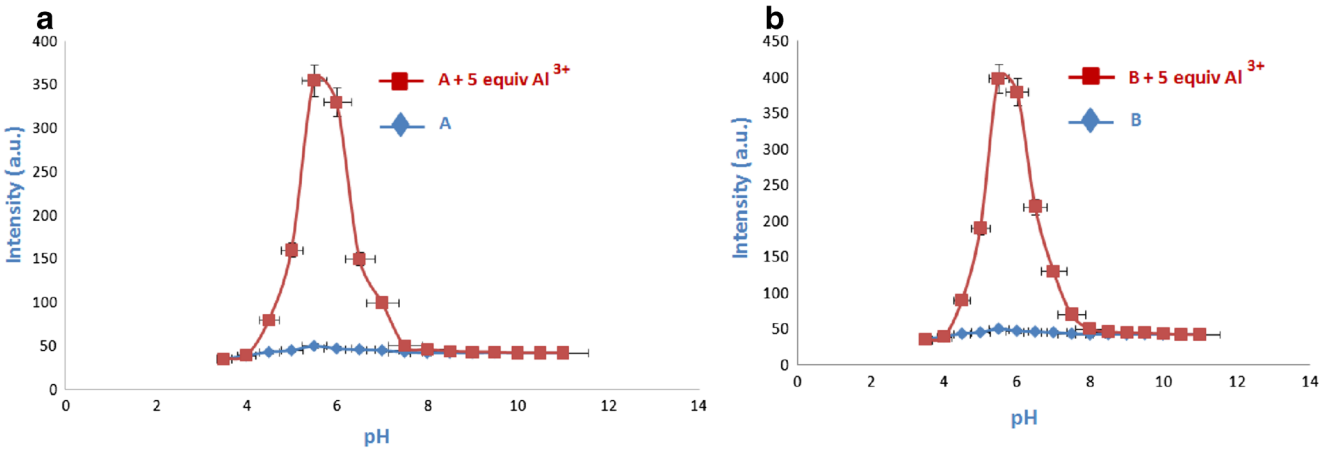

Fig. 4 (a) pH dependence of emission intensity of **A** (10 μM) in 10 mM hexamine buffer in the presence and absence of Al^{3+} (5 equiv) and (b) **B** (10 μM) in 10 mM hexamine buffer in the presence and absence of Al^{3+} (5 equiv)

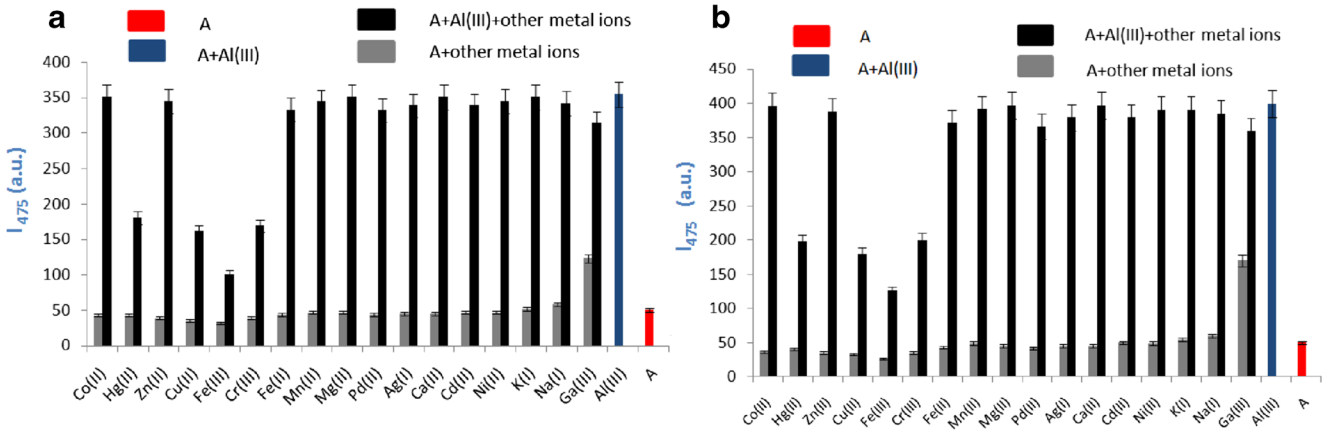

Fig. 5 Fluorescence interference test in 10 mM hexamine buffer at pH 5.5. (a) Fluorescence emission of **A** (20 μM) in the absence and presence of metal ions (250 μM). (b) Fluorescence emission of **B** (20 μM) in the absence and presence of metal ions (250 μM)

selectivity of the probes. It is to be noted that only high concentrations of Cr^{3+}, Hg^{2+}, Fe^{3+} and Cu^{2+} caused fluorescence quenching and for concentrations lower than 170 μM, no metal ions could greatly quench fluorescence emission. The quenching appeared by these four metal ions results from their inherent paramagnetic quenching effects and this quenching is not exclusive to the chemosensors **A** and **B** but common to almost all chemosensors. In the case of Cu^{2+}, no considerable quenching happened up to a concentration of 170 μM. For Hg^{2+} and Cr^{3+}, the required concentrations for quenching were nearly 180 and 210 μM, respectively. In the case of Fe^{3+}, a pronounced quenching appeared for concentrations higher than 240 μM. Generally, except for these four metal ions with concentrations over 170 μM, neither **A** nor **B** is affected by interference from competing metal ions. It is worth noting that Hg ions demonstrate a "heavy metal" effect resulting in fluorescence quenching. Moreover, the fluorescence of the Al-sensor complex quenches in the presence of Cr^{3+}, Hg^{2+}, Fe^{3+} and Cu^{2+} ions probably due to their paramagnetic property. Indeed, competitive non-radiative decay of the mixed fluorophore/metal ππ*/dd state isoenergetic to fluorophore-localized ππ* state caused this effect [51–56].

Binding mode and detection mechanism

According to ESI-mass spectrometry data (ESM Figs. S3 and S4), two new peaks at 506.5 (m/z) and 885.1 (m/z) (corresponding to $[\mathbf{A}\text{-}2H^{+}+Al^{3+}]^{+}$ and $[\mathbf{B}\text{-}2H^{+}+Al^{3+}]^{+}$, respectively) appeared upon addition of 5 equiv of Al^{3+} to **A** (200 μM) and **B** (200 μM) in H_2O. These results suggest that both chemosensors tend to form 1:1 complex with Al^{3+}. To further investigate the binding stoichiometry, a job's plot analysis was performed. Figure 6 displays 1:1 binding stoichiometry for **A** and **B** with Al^{3+}.

The ^{1}H NMR measurements were performed to determine the chemical shifts of peptides and their complexes. Based on the ^{1}H NMR evidence, the addition of 1 equiv of Al^{3+} to **A** causes a notable downfield shift (0.14 ppm) in E_1 and E_2 hydrogens (diastereotopic hydrogens of the carbons alpha to the hydroxyl group) as well as a downfield shift of 0.1 ppm in I_1, I_2, L_1 and L_2 (diastereotopic hydrogens of the carbons alpha to the carboxylate group). The addition of 1 equiv of Al^{3+} to **B** also brings about a downfield shift of 0.1 ppm corresponding to P_1, P_2, I_1, I_2, U_1 and U_2 (diastereotopic hydrogens of the carbons alpha to the carboxylate groups). After

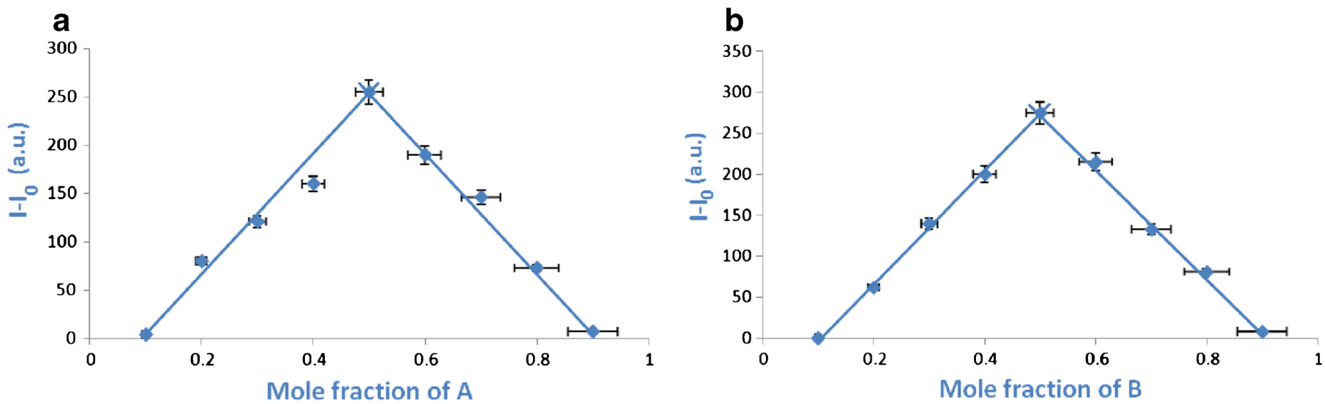

Fig. 6 (a) Job's plot for determining stoichiometry of **A** (10 μM) in 10 mM hexamine buffer at pH 5.5 with Al^{3+} (10 μM) and (b) **B** (10 μM) in 10 mM hexamine buffer at pH 5.5 with Al^{3+}(10 μM)

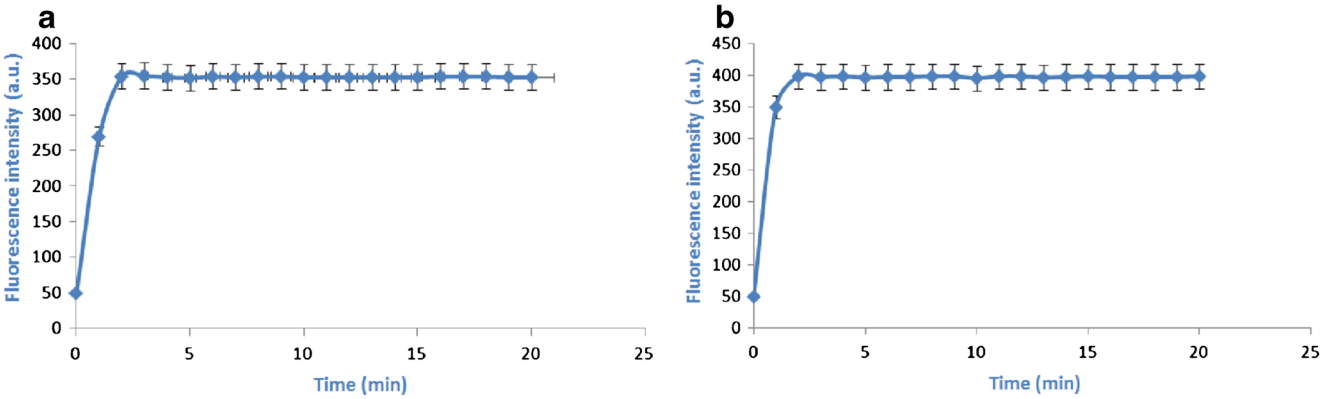

Fig. 7 Time-dependent fluorescence intensity changes of the chemosensors (10 μM) upon addition of Al^{3+} (50 μM) in 10 mM hexamine buffer at pH 5.5. (a) Kinetics of fluorescence enhancement of **A** after addition of aluminium ions. (b) Kinetics of fluorescence enhancement of **B** after addition of aluminium ions

complexation with Al^{3+}, oxygens of Ser hydroxyl moiety and carboxylate groups gain positive charge that leads to intensified withdrawing inductive effect (ESM Fig. S9).

Based on the ICT mechanism, if the amino group of 2-amino benzoyl as the electron-donating group bound to Al^{3+} ions, emission intensity would be quenched. From ESM Fig. S9, however, one can notice the more deshielded aromatic protons of **B**-Al and **A**-Al compared to those of **A** and **B** which reflects the fact that the oxygen on the amide group attached to the benzene moiety interacts with aluminium ions which would strengthen its withdrawing ability.

In this study, both chemosensors exhibited turn-on responses. To confirm that ICT is responsible for turn-on responses, ORCA software (version 4.0) was employed. The energy of HOMO and LUMO of **A**, **B**, Al^{3+} bound **A** and Al^{3+} bound **B** was calculated using B3LPY function with LANL2DZ basis set for aluminium atom and 631G (d,P) basis set for other atoms [57–59]. The electron density of HOMOs of **A**-Al and **B**-Al was delocalized along the fluorophore. However, the electron density of LUMOs of **A**-Al and **B**-Al was more localized at the fluorophore than that of **A** and **B**. These HOMO-LUMO transitions are indicative of ICT character of the probes. Furthermore, according to lower HOMO-LUMO gap of **A**-Al and **B**-Al compared with that of **A** and **B**, the formation of stable aluminium complexes is confirmed [60] (ESM Fig. S16).

Reversibility test

The reversibility of **A** and **B** was assayed in the presence of excess amounts of chelating agents, EDTA, potassium citrate and deferiprone. Excess amounts of EDTA (15 equiv) could remove Al^{3+} from the complex, returning the spectrum back to the aluminium free spectrum with an intensity of approximately 70. Deferiprone and potassium citrate as other aluminium chelating agents were tested as well. Excess amounts of either of which (15 equiv) were also added. However, they did not have the same effect, nominally quenching fluorescence and **A**-Al and **B**-Al continued to emit intense emission (ESM Figs. S17 and S18). The complete removal of Al^{3+} from the **A** and **B** by EDTA confirms the reversible sensing ability of these chemosensors towards aluminium ions [61–64].

The response time of A and B

The response time of sensors **A** (10 μM) and **B** (10 μM) was investigated in the presence of Al^{3+} (50 μM) in 10 mM hexamine buffer at pH 5.5 as shown in Fig. 7. The fluorescence intensities of **A** and **B** instantly increase to the maximum after the addition of aluminium ions in less than 2 min. From Fig. 7, one can see that within the first 2 min, the slope of the curve is steeper for **B**-Al compared with **A**-Al and within the first minute, the intensity of **B**-Al reaches up to 87.7% of its maximum and **A**-Al reaches up to 76.06% of its maximum, meaning that within the first minute, **B**-Al displays the faster response. Both chemosensors exhibit the highest intensity in less than 2 min, indicating that they are ideal sensors for the fast detection of aluminium ions [65, 66].

Conclusion

To sum up, two fluorescent peptides as novel chemosensors were synthesized. The resultant peptide-Al^{3+} complexes exhibited significant turn-on fluorescence responses based on ICT mechanism. Both chemosensors afforded detection limits lower than the previously reported Al^{3+} selective peptide-based probes. Both **A** and **B** exhibited high selectivity and sensitivity towards aluminium ions and could successfully sense Al^{3+} among seventeen competing metal ions in 100% aqueous solutions. According to the experimental tests, high binding constant (**A**-Al: 1.3029×10^4 M^{-1}, **B**-Al: 1.7586×10^4 M^{-1}) and low detection limit (**A**: 195 nM, **B**: 155 nM) were achieved. High water solubility, facile synthesis, high

overall yield and high sensitivity are the good points of **A** and **B**. These probes caused approximately 8-fold enhancement that highlights their role as ideal analytical probes for detection of Al^{3+}. So far, a few reports on highly selective peptidyl sensors for aluminium ions have been presented. We believe that this study will inspire the development of more peptide-based chemosensors for detection of metal ions particularly Al^{3+} ions.

Supplementary Information The online version contains supplementary material available at https://doi.org/10.1007/s00216-021-03339-y.

Acknowledgements We gratefully acknowledge the Iran National Science Foundation (INSF) for financial support.

Code availability Not applicable

Author contribution Not applicable

Data availability Not applicable

Declarations

Conflict of interest The authors declare no competing interests.

References

1. Liu Y, Bi A, Gao T, Cao X, Gao F, Rong P, et al. A novel self-assembled nanoprobe for the detection of aluminum ions in real water samples and living cells. Talanta. 2019. https://doi.org/10.1016/j.talanta.2018.09.104.
2. Jisha B, Resmi M, Maya R, Varma RL. Colorimetric detection of Al (III) ions based on triethylene glycol appended 8-propyloxy quinoline ester. Tetrahedron Lett. 2013. https://doi.org/10.1016/j.tetlet.2013.05.134.
3. In B, Hwang GW, Lee KH. Highly sensitive and selective detection of Al (III) ions in aqueous buffered solution with fluorescent peptide-based sensor. Bioorg Med Chem Lett. 2016. https://doi.org/10.1016/j.bmcl.2016.07.073.
4. Inan-Eroglu E, Ayaz A. Is aluminum exposure a risk factor for neurological disorders? J Res Med Sci. 2018. https://doi.org/10.4103/jrms.JRMS_921_17.
5. Kilyén M, Forgo P, Lakatos A, Dombi G, Kiss T, Kotsakis N, et al. Interaction of Al (III) with the peptides AspAsp and AspAspAsp. J Inorg Biochem. 2003. https://doi.org/10.1016/S0162-0134(03)00027-8.
6. Walton J. An aluminum-based rat model for Alzheimer's disease exhibits oxidative damage, inhibition of PP2A activity, hyperphosphorylated tau, and granulovacuolar degeneration. J Inorg Biochem. 2007. https://doi.org/10.1016/j.jinorgbio.2007.06.001.
7. Banerjee S, Brandão P, Saha A. A robust fluorescent chemosensor for aluminium ion detection based on a Schiff base ligand with an azo arm and application in a molecular logic gate. RSC Adv. 2016. https://doi.org/10.1039/C6RA21217D.
8. Nayak P. Aluminum: impacts and disease. Environ Res. 2002;89. https://doi.org/10.1006/enrs.2002.4352.
9. Platteau O, Carrillo M. Determination of metallic elements in crude oil-water emulsions by flame AAS. Fuel. 1995. https://doi.org/10.1016/0016-2361(94)00002-9.
10. Gupta VK, Singh L, Singh R, Upadhyay N, Kaur S, Sethi B. A novel copper (II) selective sensor based on dimethyl 4, 4′(o-phenylene) bis (3-thioallophanate) in PVC matrix. J Mol Liq. 2012. https://doi.org/10.1016/j.molliq.2012.07.016.
11. Gupta VK, Goyal RN, Sharma RA. Comparative studies of neodymium (III)-selective PVC membrane sensors. Anal Chim Acta. 2009. https://doi.org/10.1016/j.aca.2009.05.031.
12. Yola ML, Gupta VK, Eren T, Şen AE, Atar N. A novel electro analytical nanosensor based on graphene oxide/silver nanoparticles for simultaneous determination of quercetin and morin. Electrochim Acta. 2014. https://doi.org/10.1016/j.electacta.2013.12.086.
13. Frankowski, M. Zioła-Frankowska, A. Kurzyca, I. Novotný, K. Vaculovič, T. Kanický, V. Siepak M. Siepak, Environ Monit Assess 2011. https://doi.org/10.1007/s10661-010-1859-8.
14. Gupta VK, Mergu N, Kumawat LK, Singh AK. Selective naked-eye detection of magnesium (II) ions using a coumarin-derived fluorescent probe. Sensors Actuators B Chem. 2015. https://doi.org/10.1016/j.snb.2014.10.044.
15. Wang P, Liu L, Zhou P, Wu W, Wu J, Liu W, et al. A peptide-based fluorescent chemosensor for multianalyte detection. Biosens Bioelectron. 2015. https://doi.org/10.1016/j.bios.2015.04.094.
16. Divya D, Thennarasu S. A novel isatin-based probe for ratiometric and selective detection of Hg2+ and Cu2+ ions present in aqueous and environmental samples. Spectrochim Acta A Mol Biomol Spectrosc. 2020. https://doi.org/10.1016/j.saa.2020.118796.
17. Lim MH, Lippard SJ. Metal-based turn-on fluorescent probes for sensing nitric oxide. Acc Chem Res. 2007. https://doi.org/10.1021/ar950149t.
18. Wang P, Wu J, Su P, Xu C, Ge Y, Liu D, et al. Fluorescence "on–off–on" peptide-based chemosensor for the selective detection of Cu 2+ and S 2− and its application in living cell bioimaging. Dalton Trans. 2016. https://doi.org/10.1039/C6DT03330J.
19. Neupane LN, Park JY, Park JH, Lee KH. Turn-on fluorescent chemosensor based on an amino acid for Pb (II) and Hg (II) ions in aqueous solutions and role of tryptophan for sensing. Org Lett. 2013. https://doi.org/10.1021/ol3029516.
20. Wu J, Zou Y, Li C, Sicking W, Piantanida I, Yi T, et al. A molecular peptide beacon for the ratiometric sensing of nucleic acids. J Am Chem Soc. 2012. https://doi.org/10.1021/ja2103845.
21. Joshi BP, Cho WM, Kim J, Yoon J, Lee KH. Design, synthesis, and evaluation of peptidyl fluorescent probe for Zn2+ in aqueous solution. Bioorg Med Chem Lett. 2007. https://doi.org/10.1016/j.bmcl.2007.10.008.
22. Liao C, Li F, Huang S, Zheng B, Du J, Xiao D. A specific and biocompatible fluorescent sensor based on the hybrid of GFP chromophore and peptide for HSA detection. Biosens Bioelectron. 2016. https://doi.org/10.1016/j.bios.2016.07.002.
23. Ocain TD, Rich DH. alpha.-Keto amide inhibitors of aminopeptidases. J Med Chem. 1992. https://doi.org/10.1021/jm00081a005.
24. Gupta VK, Mergu N, Kumawat LK, Singh AK. A reversible fluorescence "off–on–off" sensor for sequential detection of aluminum and acetate/fluoride ions. Talanta. 2015. https://doi.org/10.1016/j.talanta.2015.05.053.
25. Yang X, Zhang Q, Li L, Shen R. Structural features of aluminium (III) complexes with bioligands in glutamate dehydrogenase reaction system–a review. J Inorg Biochem. 2007. https://doi.org/10.1016/j.jinorgbio.2007.06.030.
26. Yang MH, Thirupathi P, Lee KH. Selective and sensitive ratiometric detection of Hg (II) ions using a simple amino acid based sensor. Org Lett. 2011. https://doi.org/10.1021/ol201683t.
27. Badugu R, Lakowicz JR, Geddes CD. Enhanced fluorescence cyanide detection at physiologically lethal levels: reduced ICT-based

signal transduction. Bioorg Med Chem Lett. 2005. https://doi.org/10.1021/ja044421i.
28. Hossain SM, Singh K, Lakma A, Pradhan RN, Singh AK. A Schiff base ligand of coumarin derivative as an ICT-based fluorescence chemosensor for Al3+. Sensors Actuators B Chem. 2017. https://doi.org/10.1016/j.snb.2016.08.093.
29. Xu Z, Xiao Y, Qian X, Cui J, Cui D. Ratiometric and selective fluorescent sensor for CuII based on internal charge transfer (ICT). Org Lett. 2005. https://doi.org/10.1021/ol0473445.
30. Jiao Y, Zhu B, Chen J, Duan X. Fluorescent sensing of fluoride in cellular system. Theranostics. 2015. https://doi.org/10.7150/thno.9860.
31. He L, Dong B, Liu Y, Lin W. Fluorescent chemosensors manipulated by dual/triple interplaying sensing mechanisms. Chem Soc Rev. 2016. https://doi.org/10.1039/C6CS00413J.
32. Gupta A, Kumar N. A review of mechanisms for fluorescent "turn-on" probes to detect Al 3+ ions. RSC Adv. 2016. https://doi.org/10.1039/C6RA23682K.
33. Cosnard F, Wintgens V. A new fluoroionophore derived from 4-amino-N-methyl-1, 8-naphthalimide. Tetrahedron Lett. 1998. https://doi.org/10.1016/S0040-4039(98)00302-5.
34. Langelaan DN, Wieczorek M, Blouin C, Rainey JK. Improved helix and kink characterization in membrane proteins allows evaluation of kink sequence predictors. J Chem Inf Model. 2010. https://doi.org/10.1021/ci100324n.
35. Casteels-Josson K, Capaci T, Casteels P, Tempst P. Apidaecinmultipeptide precursor structure: a putative mechanism for amplification of the insect antibacterial response. EMBO J. 1993. https://doi.org/10.1002/j.1460-2075.1993.tb05801.x.
36. Gennaro R, Zanetti M, Benincasa M, Podda E, Miani M. Pro-rich antimicrobial peptides from animals: structure, biological functions and mechanism of action. Curr Pharm Des. 2002. https://doi.org/10.2174/1381612023395394.
37. Raida M, Passow H. Enhancement of divalent anion transport across the human red blood cell membrane by the water-soluble dansyl chloride derivative 2-(N-piperidine) ethylamine-1-naphtyl-5-sulfonylchloride (PENS-Cl). Biochim Biophys Acta (BBA)-Biomembranes. 1985. https://doi.org/10.1016/0005-2736(85)90255-X.
38. Asfaram A, Ghaedi M, Agarwal S, Tyagi I, Gupta VK. Removal of basic dye auramine-O by ZnS: Cu nanoparticles loaded on activated carbon: optimization of parameters using response surface methodology with central composite design. RSC Adv. 2015. https://doi.org/10.1039/C4RA15637D.
39. Li C-R, Qin J-C, Wang G-Q, Wang B-D, Yang Z-Y. A novel pyrazine derivative as a "turn on" fluorescent sensor for the highly selective and sensitive detection of Al3+. Anal Methods. 2015. https://doi.org/10.1039/C5AY00200A.
40. Yu S-Y, Wu S-P. A highly selective turn-on fluorescence chemosensor for Hg (II) and its application in living cell imaging. Sensors Actuators B Chem. 2014. https://doi.org/10.1016/j.snb.2014.04.077.
41. Gupta VK, Karimi-Maleh H, Sadegh R. Simultaneous determination of hydroxylamine, phenol and sulfite in water and waste water samples using a voltammetric nanosensor. Int J Electrochem Sci. 2015;10:303–16.
42. Pearson RG. Hard and soft acids and bases, HSAB, part 1: fundamental principles. J Chem Educ. 1968. https://doi.org/10.1021/ed045p581.
43. Klopman G. Chemical reactivity and the concept of charge-and frontier-controlled reactions. Bioorg Med Chem Lett. 1968. https://doi.org/10.1021/ja01004a002.
44. Kang T, Wang H, Wang X, Feng L. A facile Zn (II) probe based on intramolecular charge transfer with fluorescence red-shift. Microchem J. 2019. https://doi.org/10.1016/j.microc.2019.05.035.
45. Li X, Sun S, Kim IJ, Son YA. Significant emission red-shift of BODIPY derivatives with strong electron-acceptor attached. Mol Cryst Liq Cryst. 2017. https://doi.org/10.1080/15421406.2017.1358018.
46. Bhatta SR, Mondal B, Vijaykumar G, Thakur A. ICT–isomerization-induced turn-on fluorescence probe with a large emission shift for mercury ion: application in combinational molecular logic. Inorg Chem. 2017. https://doi.org/10.1021/acs.inorgchem.7b01304.
47. Neupane LN, Hwang GW, Lee KH. Tuning of the selectivity of fluorescent peptidyl bioprobe using aggregation induced emission for heavy metal ions by buffering agents in 100% aqueous solutions. Biosens Bioelectron. 2017. https://doi.org/10.1016/j.bios.2017.02.001.
48. Ali I, Jain CK. Advances in arsenic speciation techniques. Int J Environ Anal Chem. 2004. https://doi.org/10.1080/03067310410001729637.
49. Srivastava SK, Gupta VK, Jain SA. PVC-based benzo-15-crown-5 membrane sensor for cadmium. Electroanalysis. 1996. https://doi.org/10.1002/elan.1140081017.
50. Gupta VK, Nayak A, Agarwal S, Tyagi I. Potential of activated carbon from waste rubber tire for the adsorption of phenolics: effect of pre-treatment conditions. J Colloid Interface Sci. 2014. https://doi.org/10.1016/j.jcis.2013.11.067.
51. Yang W, Chen X, Su H, Fang W, Zhang Y. The fluorescence regulation mechanism of the paramagnetic metal in a biological HNO sensor. Chem Commun. 2015;51:9616. https://doi.org/10.1039/C5CC00787A.
52. Panda S, Pati PB, Zade SS. Twisting (conformational changes)-based selective 2D chalcogeno podand fluorescent probes for Cr (III) and Fe (II). Chem Commun. 2011;47:4174. https://doi.org/10.1039/C1CC10425J.
53. Tan SS, Kim SJ, Kool ET. Differentiating between fluorescence-quenching metal ions with polyfluorophore sensors built on a DNA backbone. J Am Chem Soc. 2011;133:2664. https://doi.org/10.1021/ja109561e.
54. Anand T, Sivaraman G, Mahesh A, Chellappa D. Aminoquinoline based highly sensitive fluorescent sensor for lead(II) and aluminum(III) and its application in live cell imaging. Anal Chim Acta. 2015;853:596. https://doi.org/10.1016/j.aca.2014.11.011.
55. Wu Z, Zhang Y, Shi Ma J, Yang G. Ratiometric Zn2+ sensor and strategy for Hg2+ selective recognition by central metal ion replacement. Inorg Chem. 2006;45(8):3140–2. https://doi.org/10.1021/ic051589b.
56. Varnes AW, Dodson RB, Wehry EL. Interactions of transition-metal ions with photoexcited states of flavines. Fluorescence quenching studies. J Am Chem Soc. 1972;94:946–50. https://doi.org/10.1021/ja00758a037.
57. Shree GJ, Sivaraman G, Siva A, Chellappa D. Anthracene-and pyrene-bearing imidazoles as turn-on fluorescent chemosensor for aluminum ion in living cells. Dyes Pigments. 2019. https://doi.org/10.1016/j.dyepig.2018.11.061.
58. Azadbakht R, Rashidi S. A new fluorescent chemosensor for Al^{3+} ion based on Schiff base naphthalene derivatives. Spectrochim Acta A Mol Biomol Spectrosc. 2014. https://doi.org/10.1016/j.saa.2014.02.101.
59. Wang P, Wu J, Zhou P, Liu W, Tang Y. A novel peptide-based fluorescent chemosensor for measuring zinc ions using different excitation wavelengths and application in live cell imaging. J Mater Chem B. 2015. https://doi.org/10.1039/C5TB00142K.
60. Lee S, Sung DB, Kang S, Parameswaran S, Choi JH, Lee JS, et al. Development of human serum albumin selective fluorescent probe using thieno[3,2-b]pyridine-5(4H)-one fluorophore derivatives. Sensors. 2019. https://doi.org/10.3390/s19235298.
61. Zhang Y, Guan L, Yu H, Yan Y, Du L, Liu Y, et al. Reversible fluorescent probe for selective detection and cell imaging of

oxidative stress indicator bisulfite. Anal Chem. 2016. https://doi.org/10.1021/acs.analchem.6b00061.
62. Koide Y, Kawaguchi M, Urano Y, Hanaoka K, Komatsu T, Abo M, et al. A reversible near-infrared fluorescence probe for reactive oxygen species based on Te–rhodamine. Chem Commun. 2012. https://doi.org/10.1039/C2CC18011A.
63. Kontoghiorghes G. Chemical, pharmacological, toxicological and therapeutic advances of deferiprone (L1) and other iron and aluminium chelators. Arch Toxicol Suppl. 1996. https://doi.org/10.1007/978-3-642-61105-6_21.
64. Su P, Zhu Z, Wang J, Cheng B, Wu W, Iqbal K, et al. A biomolecule-based fluorescence chemosensor for sequential detection of Ag^{+} and H_2S in 100% aqueous solution and living cells. Sensors Actuators B Chem. 2018;273. https://doi.org/10.1016/j.snb.2018.06.037.
65. Zhang S, Sun T, Xiao D, Yuan F, Li T, Wang E, et al. A dual-responsive colorimetric and fluorescent chemosensor based on diketopyrrolopyrrole derivative for naked-eye detection of Fe^{3+} and its practical application. Spectrochim Acta A Mol Biomol Spectrosc. 2018;189. https://doi.org/10.1016/j.saa.2017.09.001.
66. Ding W-H, Wang D, Zheng X-J, Ding W-J, Zheng J-Q, Mu W-H, et al. A turn-on fluorescence chemosensor for Al^{3+}, F^{-} and CN^{-} ions, and its application in cell imaging. Sensors Actuators B Chem. 2015;209. https://doi.org/10.1016/j.snb.2014.11.144.